Highly efficient source for indistinguishable single photons of controlled shape

2011 New J. Phys. 13 103036

(http://iopscience.iop.org/1367-2630/13/10/103036)

New Journal of Physics
The open-access journal for physics

Highly efficient source for indistinguishable single photons of controlled shape

Peter B R Nisbet-Jones[1], Jerome Dilley[1], Daniel Ljunggren[2] and Axel Kuhn[3]

Clarendon Laboratory, University of Oxford, Parks Road,
Oxford OX1 3PU, UK
E-mail: axel.kuhn@physics.ox.ac.uk

New Journal of Physics **13** (2011) 103036 (10pp)
Received 28 July 2011
Published 26 October 2011
Online at http://www.njp.org/
doi:10.1088/1367-2630/13/10/103036

Abstract. We demonstrate a straightforward implementation of a push-button like single-photon source, which is based on a strongly coupled atom–cavity system. The device operates intermittently for periods of up to 100 μs, with single-photon repetition rates of 1.0 MHz and an efficiency of 60%. Atoms are loaded into the cavity using an atomic fountain, with the upper turning point near the cavity's mode centre. This ensures long interaction times without any disturbances induced by trapping potentials. The latter is the key to reaching deterministic efficiencies as high as obtained in probabilistic photon-heralding schemes. The price to pay is the random loading of atoms into the cavity and the resulting intermittency. However, for all practical purposes, this has a negligible impact as an individual atom may emit up to 100 successive photons.

Due to the large number of possible applications in quantum information processing, networking, and cryptography, deterministic single-photon sources are of prime importance [1]. The ideal system is one capable of producing narrowband and indistinguishable photons on demand. For easy networking the source should also be able to absorb single photons, mapping

[1] J Dilley and P Nisbet-Jones have both equally contributed to this work.

[2] Present address: Department of Applied Physics, KTH—Royal Institute of Technology, 106 91 Stockholm, Sweden.

[3] Author to whom any correspondence should be addressed.

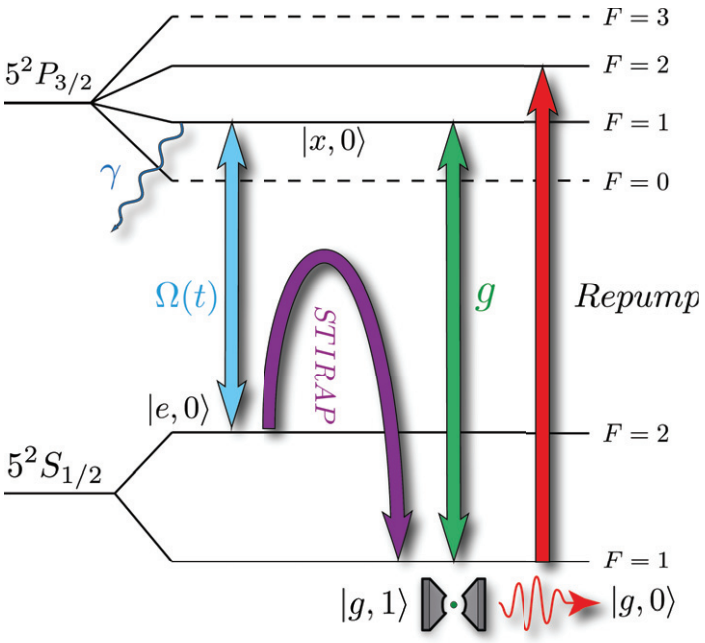

Figure 1. Schematic diagram of the energy levels of the ^{87}Rb D_2 line used for single-photon production. The atomic states $|e\rangle$, $|x\rangle$, $|g\rangle$ are involved in the STIRAP process and $|0\rangle$, $|1\rangle$ denote the intra-cavity photon number.

the photonic qubit onto the source where it can be stored for later use [2]. Due to its deterministic nature and the controllable coupling of a static qubit to a flying qubit, we have chosen to use an atom–cavity system based on a vacuum stimulated Raman process (V-STIRAP) to produce single photons. For an overview of the entire field please see [3] and the references therein. Other approaches include ions and quantum dots in cavities [4, 5], electromagnetically induced transparency (EIT) [6], and heralded down-conversion sources [7].

In order to perfect neutral atom–cavity sources many techniques have been developed. These range from intra-cavity dipole traps [8] to the feedback control of the motion of single atoms [9]. While enormous strides have been made, this has come at the cost of great experimental complexity. In addition to this complexity, the electric and magnetic fields used to create long term traps for single atoms distort the atomic levels, reducing the photon emission probability and introducing additional dephasing. With precision spectroscopy of the atom–cavity system and complete control of the atom's position using blue 'anti-trapping' dipole traps, it should be possible to overcome these distortions, although at the cost of yet further experimental complexity. We have taken a different approach and use un-trapped atoms to circumvent these difficulties, and have demonstrated high efficiency photon production with an atom–cavity interaction time which is 'long enough' for all practical purposes.

Photons are produced using a V-STIRAP process [10, 11]. Figure 1 illustrates the level scheme for the ^{87}Rb D_2 line ($5^2S_{1/2} \rightarrow 5^2P_{3/2}$). A single atom, located in a high finesse optical cavity with photon number $|n\rangle = |0\rangle$, is prepared in the $F = 2$ hyperfine ground state denoted by $|e\rangle$. The cavity is resonant with the transition $F = 1 \rightarrow F' = 1$, $|g\rangle \rightarrow |x\rangle$, and the cavity vacuum state causes an electric dipole interaction with strength g. The atom is driven with a laser on the $F = 2 \rightarrow F' = 1$, $|e\rangle \rightarrow |x\rangle$ transition with time-dependent Rabi frequency $\Omega(t)$.

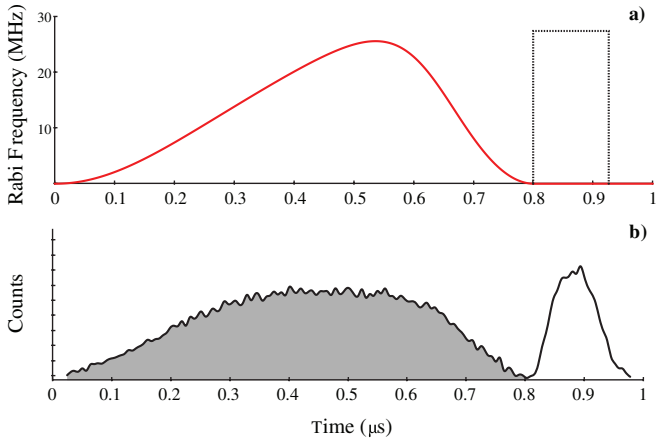

Figure 2. (a) The sequence of driving pulse (solid) and re-pump pulse (dashed). The Rabi frequency of the repump pulse is not to scale. (b) Histogram of detector clicks: STIRAP photons are shaded grey. The counts during the repump phase (unshaded) are mostly due to the beam clipping the cavity mirrors.

This combination of fields has the result of pumping the atom from $|e\rangle \rightarrow |g\rangle$ while creating a photon in the cavity mode, $|e, 0\rangle \rightarrow |g, 1\rangle$. The photon decays out of the cavity with rate 2κ. Throughout the process the atom remains in a superposition of the two ground states $|e\rangle$ and $|g\rangle$ while the excited state $|x\rangle$, which is subject to spontaneous emission γ, remains dark. Once the system has decayed to the state $|g, 0\rangle$ it is decoupled from further evolution, and must be optically pumped to the state $|e, 0\rangle$ before another photon can be emitted. This is achieved by a second laser pulse driving the atom from state $F = 1 \rightarrow F' = 2$, from which it decays probabilistically to $F = 2$. The experimental sequence of pulses is shown in figure 2.

One of the main challenges in CQED experiments is reliably coupling a single atom to an on-resonance cavity. To reduce experimental complexity we have completely removed the intra-cavity traps commonly used to achieve this. Instead we use a magneto-optical trap (MOT) and an atomic fountain to ballistically launch atoms into the cavity mode. The atom number is kept sufficiently low such that the probability of two launched atoms entering the cavity mode at the same time is negligible (less than 0.26% of all atom–cavity interactions occur with two atoms).

Around 10^6 atoms are prepared in a standard six-beam MOT approximately 8 mm below the centre of the cavity mode, as shown in figure 3. This loading phase lasts for $\approx$75 ms and is assisted by UV light-induced desorption (LIAD), allowing for fast loading rates with a relatively low background pressure of 10^{-10} mbar. Following this, the MOT coils are switched off and the frequencies of the upper and lower molasses beams are detuned relative to each other. The atoms are cooled into a moving rest frame, the velocity of which is given by

$$v = \sqrt{2}\lambda\Delta f, \tag{1}$$

where Δf describes the relative beam detuning between the upper and lower beams and λ the laser wavelength. Fine control over the frequencies of these beams (tens of kHz) leads to intrinsically fine control over the launching velocity. Varying the velocity of the launch allows the throw to be tuned so that the turning point of the atomic motion is in the cavity mode. Using simple ballistic flight arguments, and assuming a cavity mode diameter of $d = 40\,\mu$m one

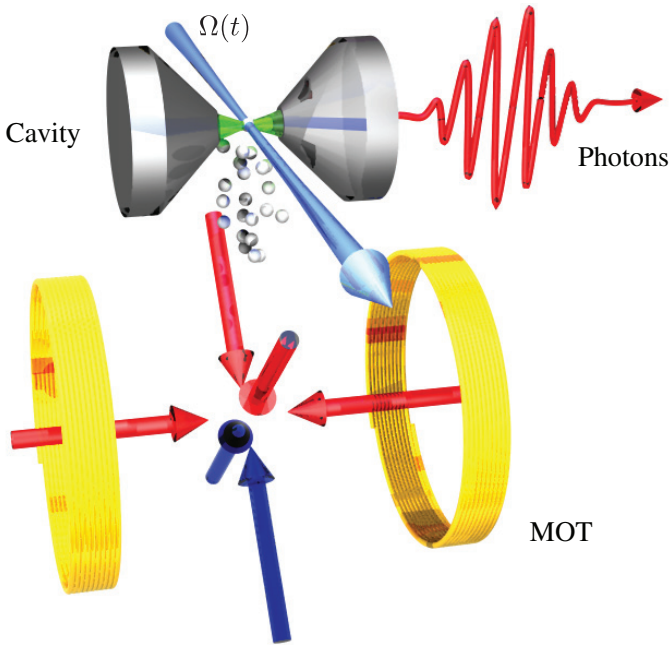

Figure 3. Artist's view of the arrangement of the cavity and MOT. The lower MOT beams are blue detuned relative to the upper to launch the atoms the 8 mm between the MOT and the cavity mode. Once in the cavity mode the atoms are driven by a Raman laser to produce single photons. The colours correspond to those in figure 1.

could, in theory, achieve maximum interaction times of $t_{\rm int} = 2\sqrt{2d/g} \approx 4$ ms. This however assumes that the atom perfectly traverses an anti-node of the cavity field with zero horizontal velocity. The finite size and temperature of the atom cloud limits the achievable interaction time to hundreds of microseconds.

The cavity is constructed from two highly reflecting mirrors separated by a distance of 74 μm. A cavity finesse of $\mathcal{F} = 85\,000$ is achieved resulting in parameters of $(g, \kappa, \gamma) = 2\pi \times (12, 12, 3)$ MHz, putting the atom–cavity system into the regime of strong coupling. The cavity was initially built using two mirrors of different transmissions $(T_1, T_2) = (40, < 1)$ ppm and losses of 2 ppm, which resulted in a finesse of $\mathcal{F} > 100\,000$ and a large asymmetry so that 96% of photons emitted into the cavity could be collected from the same spatial mode. The reduction in finesse occurred during the bake-out of the vacuum system.

The design of the cavity is intended to be both simple and inherently stable, while allowing for very good optical access. Both mirrors sit in ceramic mounts glued to shear piezo actuators (Noliac—CSAP03) which are glued to a non-magnetic stainless steel mount inside an ultra-high vacuum (UHV) vacuum chamber. High passive stability is observed with several seconds required for the cavity frequency to drift by its HWHM (12 MHz). Active feedback is achieved using the Pound–Drever–Hall technique and proportional–integral–differential (PID) regulator, allowing the cavity to be locked to the atomic resonance for many hours. The lock can be interrupted using a sample and hold integrated circuit (National Semiconductor $LF398$) during experimental runs: this allows the locking beam to be switched off while the passive stability ensures that the cavity remains on resonance for the 20 ms required for the atom cloud to pass through the cavity.

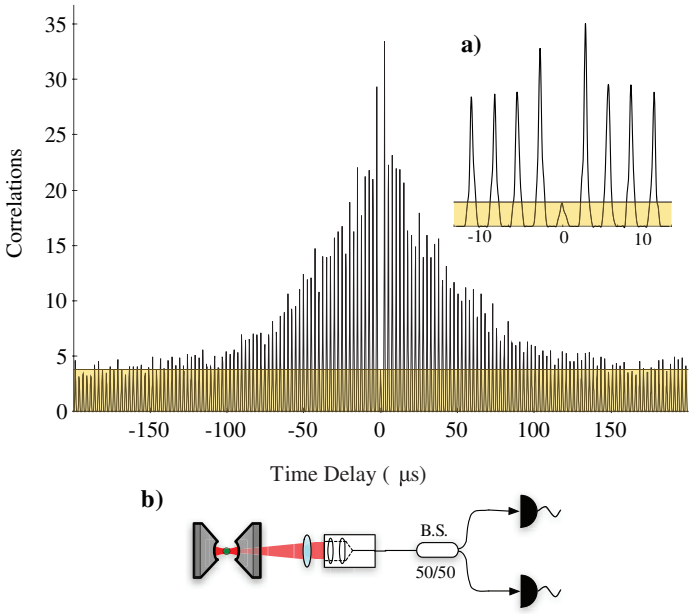

Figure 4. Second-order correlation function of the detected photons. The dark-count background level is shaded yellow. The missing central peak implies a single-photon source, and the envelope of the peaks implies that the atom remains in the cavity for 100 μs. Insets show a zoomed in view around $\tau = 0$ (a) and the interferometer setup (b).

To verify that we are producing single photons, the photon stream is interrogated using a Hanbury–Brown–Twiss-type interferometer. A 50/50 beam splitter is placed in the beam path and correlations between the clicks on each of the two output ports are measured. This can be used to calculate the second-order intensity correlation function of the emitted photons. The cross-correlation of the photodetectors D1 and D2 is shown in figure 4, which is defined as

$$g^{(2)}(\tau) = \frac{\langle P_{\mathrm{D1}}(t) P_{\mathrm{D2}}(t-\tau)\rangle}{(\langle P_{\mathrm{D1}}(t)\rangle \langle P_{\mathrm{D2}}(t)\rangle)}, \tag{2}$$

where $P_{\mathrm{D1}}(t)$ and $P_{\mathrm{D2}}(t)$ are the probabilities of detecting a photon at the corresponding detector [12]. This function includes both photon correlations and contributions from the dark noise of the detectors (1 kHz) . Detector counts which occur during the optical repumping have been omitted; see figure 2(b). This masking gives rise to the periodicity of the background which would otherwise be at a constant level (shown in yellow shading, with a negligible two atom contribution). The $g^{(2)}(\tau)$ function exhibits the periodicity that one would expect for a pulsed source, with peaks separated by the repetition period. It can clearly be seen that the expected peak at $\tau = 0$ is missing. This demonstrates that there is only one photon produced per atom per pulse. The envelope of the $g^{(2)}(\tau)$ correlation function is a consequence of the limited atom–cavity interaction time. At 100 μs this allows for the implementation of many interesting QIP schemes, e.g. entanglement generation, teleportation and gate operations [13–15].

A typical histogram of the photon arrival times is shown in figure 5(a). When an atom passes through the cavity the average photon count rate increases sharply—this can clearly be seen by the red bars. Post selection of these atom transit events allows for the efficiency of the

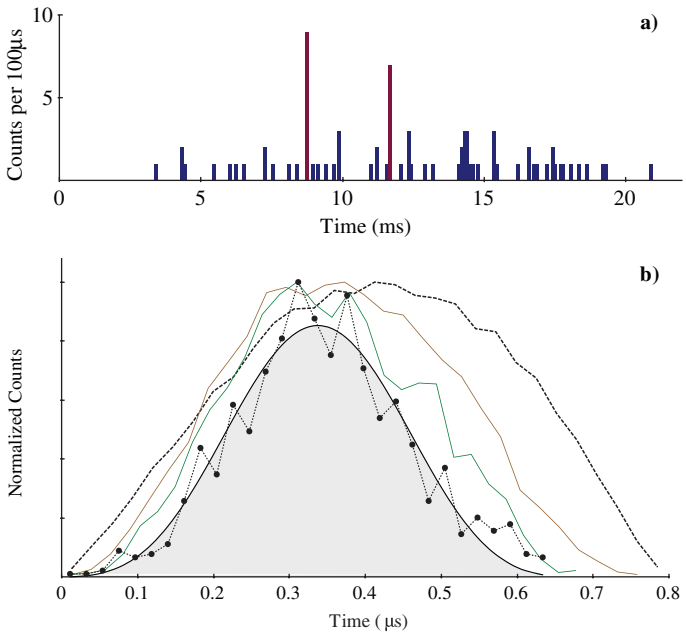

Figure 5. (a) Histogram of photon arrival times, binned with the interaction time. Time bins in which an atom passes through the cavity are highlighted in red. By post-selecting these time bins the $|\psi(t)|^2 = \sin^4(t)$ shape (shaded) for a well coupled atom can be recovered (b). The photon shapes are shown when not post-selecting (dashed), and selecting only photon which occur with more than 3 (brown), 5 (green) and 7 (circle) counts per bin.

photon production process for a well coupled atom to be determined. The emission probability is calculated by conditioning on a detector click and then looking for clicks in the subsequent pulses. The emission probability P is observed to change as the atom moves through the cavity as the coupling g depends on the atom's position within the mode.

As the most likely place for the atom to emit a photon is at the cavity centre, calculating the efficiency by looking at the probability of emitting two successive photons will always underestimate P; the atom will have moved away from the mode centre where it experiences the maximum atom–cavity coupling strength, g_0, when the second emission takes place. Instead, we map the change in P with multiple successive pulses which follows a Gaussian curve. It is possible to extrapolate this curve back to the origin to estimate the maximum single-photon emission probability $P_{\max}$. We find a detector click probability of $15 \pm 2\%$. By including the detector quantum efficiency of 70 and a 65% collection efficiency (coupling photons into to the fibre, optical losses and losses from the vacuum chamber viewport) this corresponds to a maximum photon emission probability of $33 \pm 3.5\%$. As previously intimated, during the vacuum bakeout a dirty Rb dispenser caused the mirror losses to increase from 2 ppm $\rightarrow$ 18 ppm. This reduced the photon out-coupling efficiency from 96% to only 50%. Including this factor in the calculation gives the photon production probability inside the cavity, $P_{\max} = 66 \pm 7\%$.

The pulse applied to the atom was calculated to produce a $\psi(t) = \sin^2(t)$ shape using the method in [16], having assumed a stationary atom experiencing the maximum coupling strength

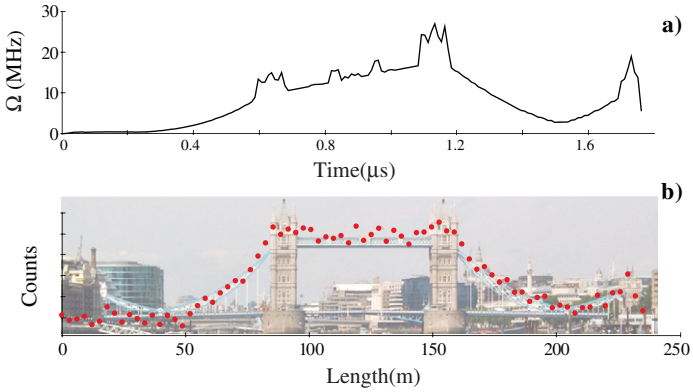

Figure 6. (a) Driving pulse applied to an atom to obtain a photon with the shape shown below. The actual pulse was significantly smoothed due to the limited AOM bandwidth. (b) Spatial profile of the photon's probability density, reconstructed from the measured detection-time histogram. This has been done assuming that the light propagates in a fibre with a refractive index of $n = 2$. Any resemblance to iconic landmarks is intentional.

g_0. In reality, due to the imperfect positioning of the atom within the cavity mode, the atom will experience coupling strengths over the full range of $g = 0 \rightarrow g_0$. The grey shaded area in figure 2(b) shows a histogram of the photon arrival times from the beginning of the driving pulse (from a total of 10^5 photon counts). This clearly deviates from an ideal $\psi(t) = \sin^2(t)$ envelope and is due to photon emission from poorly coupled atoms.

The post selection used to determine the emission probability can also be used to recover the shape of the photons being produced. By selecting out only the photons from well coupled atoms the measured shape collapses to the expected $\psi(t) = \sin^2(t)$, as shown in figure 5(b).

It is also possible to engineer the photon's shape in more interesting ways. By tailoring the Rabi frequency of the driving laser it is possible to force the photon amplitude to follow, for example, the shape of Tower Bridge in London, as shown in figure 6. The shaping is fundamentally limited by the atom–cavity coupling g_0 and cavity decay κ; however, in practice this is limited by the AOM bandwidth (5 MHz) used to modulate the driving pulse's amplitude.

The indistinguishability of the emitted photons can be tested using a Hong–Ou–Mandel (HOM) interferometer [17]. By introducing an optical delay, two photons from successive pulses are overlapped on a beam-splitter (BS). In the case where they are identical bosons they will coalesce and leave the BS through the same output port: for a perfect source, simultaneous detection at detectors 1 and 2 should not occur. As the temporal resolution of the detectors (350 ps) is much shorter than the photon length, one can also observe the beat of the two photons [18]. In a non-temporally resolved HOM interferometer, the temporal overlap of the photons on the BS is varied and the resultant correlations plotted. In this time-resolved case, the photons are always perfectly overlapped and the correlations instead vary with the time difference between clicks on the two detectors $\delta\tau$. The theoretical background is set out in [19, 20].

The cross-correlation between the two detectors is shown in figure 7(a) for parallel (red) and perpendicular (blue) polarization, and the interferometer is shown in figure 7(b). With parallel polarization the two photons interfere and correlations should not occur, whereas

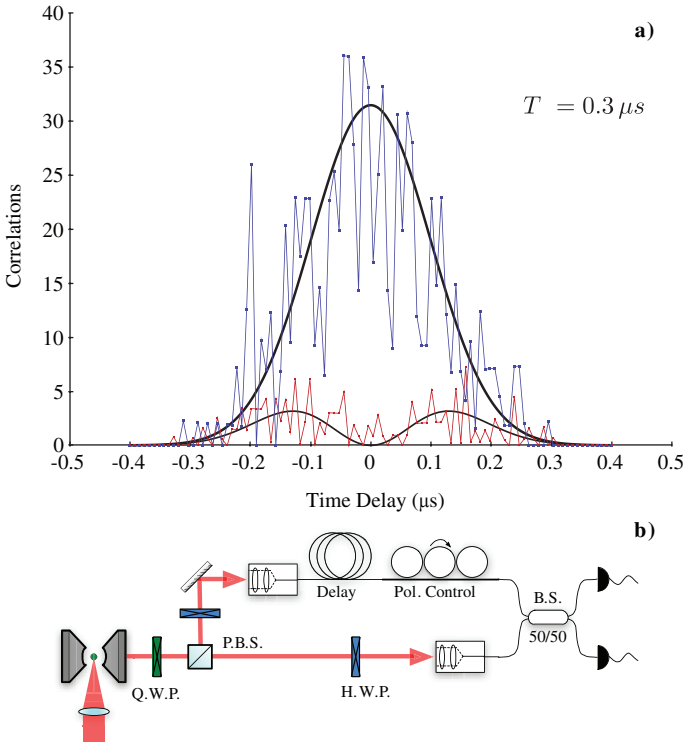

Figure 7. (a) Cross correlation function of detectors 1 and 2, demonstrating two-photon interference for photons overlapping spatially and temporally on a BS. Perpendicular polarized photons are shown in blue and parallel polarized photons in red. (b) The interferometer setup. A 200 m long fibre is used to delay one photon such that it can be overlapped with the subsequently emitted one. A fibre-based BS and polarization optics are used to ensure near-perfect spatial and polarization overlap.

with perpendicular polarization they do not interfere and a correlation function given by the convolution of the shapes of the two photons is observed.

As expected, the number of correlations for parallel polarization is greatly reduced compared to the perpendicular case. In addition, a pronounced dip at $\delta\tau = 0$ is visible, the width of which is governed by a characteristic 'coherence time' $T = 300 \pm 40$ ns. This coherence time is limited by a dephasing between the two photons at rate $\Delta\omega = 1/(2T) = 2\pi \times 265$ kHz, and is primarily explained by the stability of the pumping laser and stray magnetic fields, which each cause a broadening in the range of 100–200 kHz. We also note that spontaneous emissions within the atom might give rise to dephasing. Numerical calculations show that these occur with a probability of less than 2% per successful photon emission, which is below the noise floor. Furthermore, we observed a negligible change in the HOM signal in an unconditional analysis of the data. This is easily explained as the probability for emission of successive photons scales with P^2, which is close to zero unless an atom is well coupled.

We define the visibility $V_{2\mathrm{ph}}$ of the HOM signal as the reduction in the areas of the correlation curves between the completely distinguishable and completely indistinguishable

case:

$$V_{2\mathrm{ph}} = 1 - \frac{\int \Phi_{\parallel}(\tau)\,\mathrm{d}\tau}{\int \Phi_{\perp}(\tau)\,\mathrm{d}\tau}. \tag{3}$$

This is the time-resolved equivalent of looking at the depth of the $\tau = 0$ dip in non time-resolved HOM—the extra information is simply averaged away. The overall extinction ratio for the photon is $V_{2\mathrm{ph}} = 0.87 \pm 0.05$.

In summary, we have demonstrated a cavity-based, deterministic single-photon source. Emission rates of 1 MHz can be achieved, and the lack of disturbances caused by trapping fields means the source exhibits efficiencies of over 60%. Despite the lack of a trap, atoms remain inside the cavity mode for up to 100 μs giving enough time for QIP operations to be performed [13]. The emitted photons show very strong anti-bunching and an indistinguishability leading to a HOM visibility of 87%. We have also shown control over the shape of the photon's wavefunction, a requirement for an effective quantum memory [21–23]. The experimental arrangement is simple and thus more readily reproducible than similar sources, and therefore shows great promise for testing the individual nodes from which a scalable quantum network will be composed.

Acknowledgments

This work was supported by the Engineering and Physical Sciences Research Council (QIP IRC and EP/E023568/1), the Deutsche Forschungsgemeinschaft (Research Unit 635), and the EU through the RTN EMALI (MRTN-CT-2006-035369). We are grateful to G Langfahl-Klabes for his help in the early stages of this work.

References

[1] Kimble H J 2008 The quantum internet *Nature* **453** 1023
[2] Boozer A D, Boca A, Miller R, Northup T E and Kimble H J 2007 Reversible state transfer between light and a single trapped atom *Phys. Rev. Lett.* **98** 193601
[3] Kuhn A and Ljunggren D 2010 Cavity-based single-photon sources *Contemp. Phys.* **51** 289
[4] Keller M, Lange B, Hayasaka K, Lange W and Walther H 2004 Continuous generation of single photons with controlled waveform in an ion-trap cavity system *Nature* **431** 1075
[5] Moreau E, Robert I, Gérard J-M and Abram I 2001 Single-mode solid-state single photon source based on isolated quantum dots in pillar microcavities *Appl. Phys. Lett.* **79** 2865
[6] Chanelière T, Matsukevich D N, Jenkins S D, Lan S Y, Kennedy T A B and Kuzmich A 2005 Storage and retrieval of single photons transmitted between remote quantum memories *Nature* **438** 833
[7] Mosley P, Lundeen J, Smith B, Wasylczyk P, U'Ren A, Silberhorn C and Walmsley I A 2008 Heralded generation of ultrafast single photons in pure quantum states *Phys. Rev. Lett.* **100** 133601
[8] Puppe T, Schuster I, Grothe A, Kubanek A, Murr K, Pinkse P W H and Rempe G 2007 Trapping and observing single atoms in a blue-detuned intracavity dipole trap *Phys. Rev. Lett.* **99** 013002
[9] Kubanek A, Koch M, Sames C, Ourjoumtsev A, Pinkse P W H, Murr K and Rempe G 2009 Photon-by-photon feedback control of a single-atom trajectory *Nature* **462** 898
[10] Kuhn A, Hennrich M and Rempe G 2002 Deterministic single-photon source for distributed quantum networking *Phys. Rev. Lett.* **89** 067901
[11] Hennrich M, Legero T, Kuhn A and Rempe G 2000 Vacuum-stimulated Raman scattering based on adiabatic passage in a high-finesse optical cavity *Phys. Rev. Lett.* **85** 4872

[12] Hennrich M, Legero T, Kuhn A and Rempe G 2004 Photon statistics of a non-stationary periodically driven single-photon source *New J. Phys.* **6** 86
[13] Himsworth M, Nisbet P, Dilley J, Langfahl-Klabes G and Kuhn A 2011 EIT-based quantum memory for single photons from cavity-QED *Appl. Phys.* B **103** 579
[14] Wilk T, Webster S C, Kuhn A and Rempe G 2007 Single-atom single-photon quantum interface *Science* **317** 488
[15] Olmschenk S, Matsukevich D N, Maunz P, Hayes D, Duan L M and Monroe C 2009 Quantum teleportation between distant matter qubits *Science* **323** 486
[16] Vasilev G S, Ljunggren D and Kuhn A 2010 Single photons made-to-measure *New J. Phys.* **12** 063024
[17] Hong C K, Ou Z Y and Mandel L 1987 Measurement of subpicosecond time intervals between two photons by interference *Phys. Rev. Lett.* **59** 2044
[18] Legero T, Wilk T, Hennrich M, Rempe G and Kuhn A 2004 Quantum beat of two single photons *Phys. Rev. Lett.* **93** 70503
[19] Legero T, Wilk T, Kuhn A and Rempe G 2003 Time-resolved two-photon quantum interference *Appl. Phys.* B **77** 797
[20] Legero T, Wilk T, Kuhn A and Rempe G 2006 Characterization of single photons using two-photon interference *Adv. At. Mol. Opt. Phys.* **53** 253
[21] Cirac J I, Zoller P, Kimble H J and Mabuchi H 1997 Quantum state transfer and entanglement distribution among distant nodes in a quantum network *Phys. Rev. Lett.* **78** 3221
[22] Specht H P, Nölleke C, Reiserer A, Uphoff M, Figueroa E, Ritter S and Rempe G 2011 A single-atom quantum memory *Nature* **473** 190
[23] Dilley J, Nisbet P, Shore B W and Kuhn A 2011 Cavity-based single-atom quantum memory arXiv:quant-ph:1105.1699v1